Rock Mech Rock Engng (2007) 40: 531–561
DOI 10.1007/s00603-007-0158-3
Printed in The Netherlands

Rock Mechanics
and Rock Engineering

Manuel Rocha Medal Recipient

Wave interaction with underground openings in fractured rock

By

M. W. Hildyard

Department of Earth and Ocean Sciences, University of Liverpool, Liverpool, UK

Received August 3 2007; Accepted October 31 2007; Published online December 4 2007

This paper summarizes some of the work from Dr. Hildyard's thesis presented during the ISRM Rocha Medal ceremony at the ISRM International Symposium, EUROCK 2005, in Brno, in May 2005. Dr. Hildyard was born in the UK, but grew up and was educated in South Africa. He received his Ph.D. from the University of Liverpool in 2002. He is currently a Research Associate at the University of Liverpool

Summary

The objective of this work is to lead to improved models of seismic wave propagation around underground openings by studying the interaction of the waves with the fractured rock surrounding these openings. It demonstrates that seismic models can help in stability problems such as rockbursting in deep-level mining, or in the interpretation of micro-fracturing at waste storage sites. A significant emphasis is placed on comparing the models with observations from controlled experiments. These comparisons demonstrate that the wave propagation can be reliably and accurately modelled, and in so doing it motivates their application to the larger rock engineering problems. Seismic wave models are first applied to laboratory experiments on multiple fractures. Simulation through multiple displacement discontinuities yields strikingly similar waveforms to the experiments, while also identifying the need to build stress dependence into the fracture models, such as stress dependent fracture stiffness. The wave-fracture modelling is

Correspondence: Dr. M. W. Hildyard, Department of Earth and Ocean Sciences, University of Liverpool, Liverpool, UK
e-mail: mark.hildyard@liverpool.ac.uk

extended to *in situ* fractures in rock at the surface of a deep tunnel, using data collected during an acoustic emission experiment at the URL Mine-by tunnel. Waveforms from the velocity scans are compared against those from elastic models and various models of fracture, such as random assemblies of small open fractures (cracks) and larger fractures with fracture stiffness. Results indicate that it is possible to account for the wave-speeds and amplitudes using models with fractures. A generic method is then proposed for calculating the frequency variation of wave-speed and amplitude for any collection of cracks. The models of fracture are then applied to the rockburst problem, to investigate how the excavation affects the amplitude and the distribution of ground motion. The results provide important insights into the causes of the apparent amplification observed by researchers in this field. The thesis also covers the theory of the models used, including novel numerical work on dispersion and new grid schemes. The full detail of the work cannot be covered in this paper which instead seeks to summarize the main achievements.

1. Introduction

This work is aimed at improving models of wave propagation around underground openings, with a particular emphasis on waves in fractured rock. There are two long-term motivations for this. The first is that such models can be used as a tool in addressing the rockburst problem in deep-level mining, where models of rockbursts can estimate the amplitudes and distribution of seismic wave motion, and hence the likely damage, around an excavation. The second motivation is that these models can be used for interpreting the state of fracturing from seismic waves. This is a very desirable capability in a number of industries, whether mining, oil extraction or nuclear waste storage. Achieving either of these goals however, requires accurate models of wave interaction with fracturing.

Rockbursts in mines are a serious hazard and are widespread in the deep hard-rock mining districts of the world. However, whereas for large earthquakes the simulation of seismic events closely coupled to comparisons with the observed near- and far-field seismograms, has been widespread for some time (e.g. Wald et al., 1991; BSSA, 1991), a similar level of analysis has not yet been achieved in rockburst research. Dynamic numerical models have been applied in a number of rockburst studies, and many calculate seismic waveforms at a distance from the event (e.g. Cundall and Lemos, 1990; Brady, 1990; Mack and Crouch, 1990; Müller, 1991; Siebrits et al., 1993; Tinucci and Spearing, 1993, Hildyard et al., 1995). In general these suffer from the deficiency of being two-dimensional analyses and in not having direct detailed comparisons between measured and modelled seismograms. Experiments in photoelastic material have demonstrated that modelled wave behaviour can closely correspond to that observed (e.g. Daehnke et al., 1996; Daehnke and Hildyard, 1997; Uenishi, 1997). Again, these are for two-dimensional analyses and with a more ideal elastic material than is typical of a rockmass. Some three-dimensional analyses have been performed (e.g. Handley et al., 1996; Hildyard and Milev, 2001a, b) but have not achieved fully convincing comparisons with measured waveforms from *in situ* recordings in mines – certainly not to the level at which Brady (1990) concluded, that not just the peak velocity but the full wave motion is important in determining damage. A review of previous applications of wave propagation models to the rockburst problem leads to the conclusion that there is a need for (i) three-dimensional simulation (ii) evidence of reliable simulation through comparison with observed seismograms; (iii) evidence of accurate wave propagation in the excavation's fracture zone.

The interaction of waves with fracturing has long been identified as crucial by prominent researchers in the field of rock mechanics (Cook, 1992). Much research has been conducted, with significant experimental achievements and greater understanding of the physics. A displacement discontinuity has been proposed as a suitable discrete representation of a fracture (Schoenberg, 1980; Myer et al., 1985). Experimental studies indicate that this representation captures many of the frequency-dependent effects on waves due to fracturing (Pyrak-Nolte et al., 1990a, b). An alternative approach attempts to encapsulate the effects of large numbers of fractures into the behaviour of the medium. The fractured rock is then treated as an effective elastic medium, with the elastic constants related to the density of fracturing, typically leading to anisotropy in the seismic velocities (e.g. O'Connell and Budiansky, 1974; Crampin, 1981; Sayers and Kachanov, 1991). Expressions for the effective attenuation have also been developed (Hudson, 1981; Liu et al., 2000). However, most numerical studies of waves through fractures make some of the following assumptions: two-dimensional wave-propagation; plane wave propagation; small amplitude motions; low frequencies relative to the crack-size; dilute crack concentration; uniform stress state, or are only accurate for first arrivals. Many of these assumptions are poor in the context of real problems. Wave motion is non-planar and three-dimensional analysis is essential. Excavations are in a highly non-uniform stress-field and in the case of deep-level mining, the excavation surface is highly fractured, wave amplitudes may be large, and sources are in the near-field. Microseismic and ultrasonic recordings contain frequencies which do not satisfy low frequency and plane wave assumptions, while accurate simulation is required over the full duration of dynamic motion and not just first arrivals, so that the full effect on the rockmass can be assessed.

The case studies in this work attempt to redress some of these deficiencies, showing that true three-dimensional modelling in the vicinity of excavations in complex media is now feasible. The first section briefly introduces the numerical basis for the work and highlights some of the novel numerical developments in the thesis. Results are then presented from numerical simulations of a laboratory experiment of wave propagation through multiple fractures, evaluating the practical use of the displacement discontinuity model of a fracture. Models are then applied to rock at the surface of a deep excavation with an unknown distribution of fractures, using data recorded in underground velocity surveys. Finally, the techniques are applied to the rockburst problem, studying how the excavation and fracturing influence the amplitude and distribution of ground motion.

2. Theoretical and numerical basis for models

The program WAVE was used throughout this work to model three-dimensional seismic wave propagation and its interaction with cavities and fractures. The program was authored by Cundall (1992), including the mesh scheme and the novel implementation of a discontinuity used to represent both free surfaces and fractures, and extended by Hildyard (1995) with aspects such as higher order grid accuracy and fracture intersection. WAVE solves the system of first order wave equations using finite differences on a staggered grid, a method which has been widely used in seismological applications

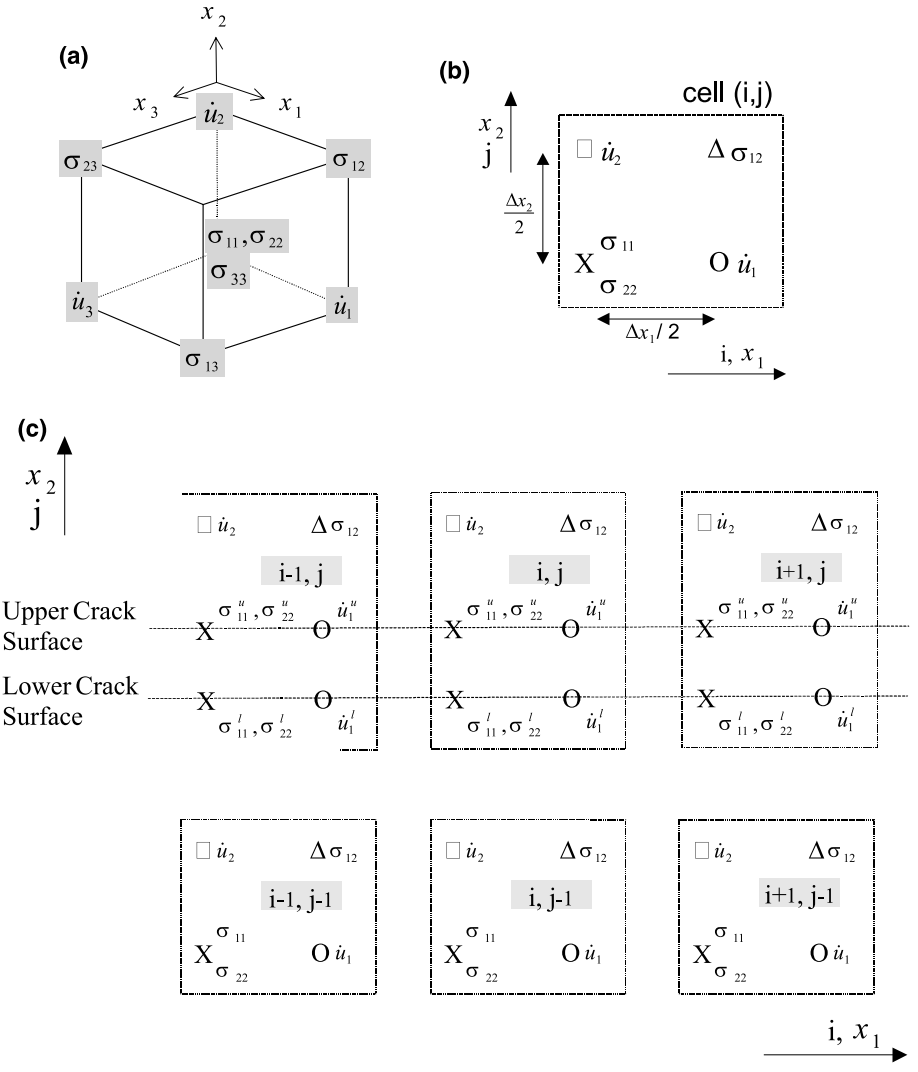

Fig. 1. The staggered grid used in WAVE. (**a**) Single cell in the 3D staggered grid showing positions of the different stress and velocity components. (**b**) Single cell in the 2D staggered grid. (**c**) Illustration (for the 2D case) of the zero-width discontinuity used to implement a crack or fracture. Upper and lower surfaces share the same nominal position in space

(Madariaga, 1976; Aki and Richards, 1980; Virieux, 1984; Graves, 1996). In this formulation, a continuum is discretized into a grid or mesh, with different components of stress and velocity computed at different positions in space. Figure 1a and b show the positions of each component within a unit cell, for three- and two- dimensions. Fundamental to the program, and to this work, is a zero-width discontinuity within the mesh. This is used to model fractures and openings. It consists of two coincident surfaces on which certain grid variables are continuous while others are discontinuous with separate

values for the upper and lower surfaces. The fracture surfaces are coupled by a normal and shear fracture stiffness. Figure 1c illustrates this discontinuity within the two-dimensional staggered mesh. A detailed description of the crack implementation is available in Hildyard (2001) or Hildyard and Young (2002).

Hildyard (2001), reviews in detail each aspect of the WAVE code, describing the staggered grid method, deriving the mesh equations, and covering the problem of numerical dispersion and fourth and higher order approximations. It also describes the implementation of fractures as a zero-width displacement discontinuity, frictional slip, crack opening-closing behaviour, crack intersections and cavities, and covers the boundary conditions used to reduce reflections and to solve for static stress states. A number of novel numerical developments were made during the course of this work. They include:- an examination of the memory and run-time efficiency of some alternatives to the staggered grid; practical methods for analysing the dispersion accuracy of numerical schemes; efficient schemes for obtaining coupled static and dynamic solutions; methods within the staggered grid scheme which allow general orientations of cracks and cavities; new finite difference schemes with comparable efficiency to the fourth order staggered grid scheme. These developments were aimed at exploring how the fracture modelling can be extended in the future to cover more complex fracture geometries while maintaining the high efficiency required for these sorts of analyses.

Two practical approaches were developed for analysing dispersion in numerical schemes. Numerical dispersion is an important problem associated with element and grid-based solutions to the wave equation. Calculating the dispersion accuracy provides a useful way of quantifying the accuracy of different grid schemes and of comparing their efficiency. The proposed practical approaches have an advantage over analytical analyses, as they allow the dispersion of a numerical scheme to be evaluated without requiring knowledge of its solution method. They can also be used to analyse complex, non-uniform meshes. The first method involves passing a plane wave through the numerical mesh and recording spatial waveforms at two different times (t_1 and t_2). The second method requires recording time waveforms at two different positions (x_1 and x_2) along the wave path. Taking Fourier transforms of these waveforms and denoting A_1 and A_2 as the amplitude and ϕ_1 and ϕ_2 as the phase functions of these transforms, expressions were obtained for phase velocity as a function of wave-number or frequency. Equation (1a) is the relationship derived for two spatial waveforms, while Eq. (1b) is the relationship derived for two time waveforms.

$$c(\gamma) = \frac{1}{\gamma(t_2 - t_1)}\left[-(\phi_2 - \phi_1) + i \ln\left(\frac{A_2}{A_1}\right)\right] \tag{1a}$$

$$c(\omega) = \omega(x_2 - x_1)\left[\frac{-(\phi_2 - \phi_1) - i \ln\left(\frac{A_2}{A_1}\right)}{(\phi_2 - \phi_1)^2 + \left[\ln\left(\frac{A_2}{A_1}\right)\right]^2}\right] \tag{1b}$$

The second method is demonstrated in Fig. 2. Figure 2a shows the time waveforms for the 2nd order and 4th order staggered grid. The extra oscillations evident in the waveforms and the loss of amplitude with distance, are due to numerical dispersion,

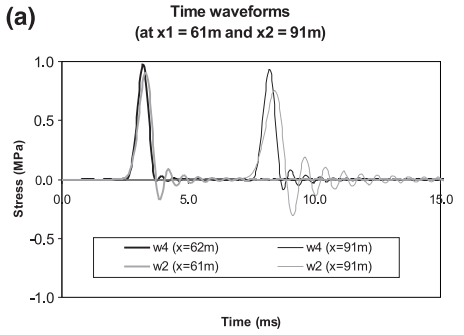

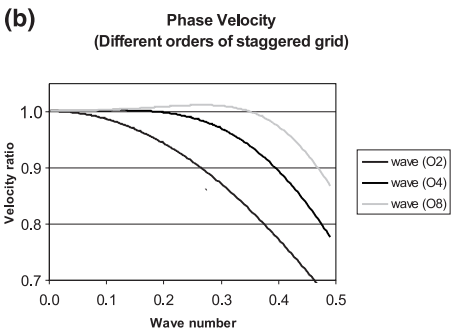

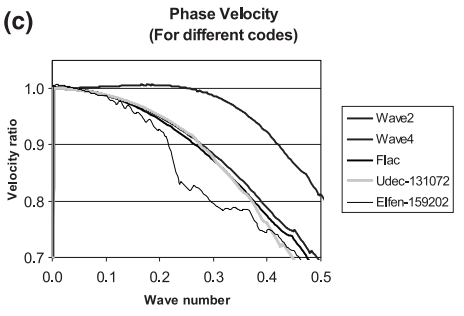

(d)

Mesh Scheme	Accuracy (Order)	Memory ratio	Run-time ratio
Wave4	(4)	1.0	1.0
Wave2	(2)	4.0	6.7
Flac	(2)	34.4	115.1
Elfen-159202	(~2)	238.0	554.9
Udec-131072	(~2)	42.8	1052.6
NuWave4	(4)	1.4	2.5

Fig. 2. Practical calculation of dispersion in numerical codes. (**a**) Time-domain waveforms collected at two different positions – near a test source and at some distance from the test source – shown for the 2nd and 4th order WAVE grid. (**b**) Phase velocity (calculated using Eq. 1b), shown for the 2nd, 4th and 8th order WAVE grid. (**c**) Phase velocity calculated for different commonly used codes (**d**) Comparison between different codes and grid schemes, for memory and run-times required to obtain the equivalent dispersion accuracy as that of a 4th order staggered grid

and the waveforms show that there is a clear advantage to the 4th order grid. Figure 2b shows the phase velocity curves calculated from these waveforms using Eq. 1b. Ideal wave propagation would result in a constant phase velocity ratio of 1. The departure from this with increasing frequency, limits the frequency range over which the numerical scheme can be meaningfully applied. The accurate frequency range in the 4th order scheme is approximately twice that of the 2nd order scheme.

Alternative finite difference and finite element schemes exist which allow complex fracture geometries. Three general-purpose codes commonly used in rock mechanics were analysed to determine their accuracy and efficiency of wave propagation. The codes studied were UDEC (Itasca, 1993a), FLAC (Itasca, 1993b) and ELFEN (Rockfield, 1999). Efficiency was determined based on the memory and run-times required to obtain the equivalent dispersion accuracy. Figure 2c shows the calculated dispersion curves while Fig. 2d tabulates efficiency results. For two-dimensions, the general-purpose codes were found to be nearly two orders of magnitude less efficient than a fourth order, regular spaced, staggered grid, in both memory requirements and run-time. These general-purpose codes would not support a sufficient number of elements to solve many of the problems dealt with in this work and more efficient schemes need to be used.

Methods were investigated for generalising the staggered grid scheme to allow for angled cracks. A second order approximation was developed for an explicit angled crack based on the approach of grid-aligned cracks. This implementation is efficient for studying limited orientations of fracturing, but is not suited for modelling general fracture geometries, and its accuracy was not formally evaluated. An approach proposed by Coates and Schoenberg (1995), using a localised distribution of transversely isotropic material to represent fractures, was also implemented, but was shown to give severely inaccurate results for angled fractures with a low fracture stiffness. A third method was to extend an approach by Hestholm and Ruud (1994), who implemented a curved free surface topography by mapping the wave equations and boundary conditions from a curvilinear mesh to a rectangular mesh. The approach was followed to derive equations for a general curved fracture, but it was noted that the implementation on a staggered grid has implications for accuracy, as certain derivatives are not readily approximated.

Novel finite-difference grid schemes were derived in an attempt to develop an efficient alternative to the fourth order staggered mesh. A family of two-dimensional schemes was investigated based on a four-noded quadrilateral element. A four-noded finite-difference scheme can be formulated in a similar manner to that of the staggered mesh and is readily given fourth order accuracy. The unit cell for this grid contains all components of stress at the σ_{11} position in Fig. 1b, and all components of velocity at the σ_{12} position in Fig. 1b. This is the same scheme proposed recently by Jianfeng (1997), but unfortunately suffers from a problem termed hour-glassing (Marti and Cundall, 1982; Molenkamp et al., 1992). The program FLAC (Itasca, 1993b) uses a

$$\dot{\sigma}_{11} = E1\frac{1}{2h}\begin{bmatrix}-1 & 1\\ -1 & 1\end{bmatrix}\dot{u}_1 + E2\frac{1}{2h}\begin{bmatrix}1 & 1\\ -1 & -1\end{bmatrix}\dot{u}_2 \tag{1a}$$

$$\dot{\sigma}_{22} = E2\frac{1}{2h}\begin{bmatrix}-1 & 1\\ -1 & 1\end{bmatrix}\dot{u}_1 + E1\frac{1}{2h}\begin{bmatrix}1 & 1\\ -1 & -1\end{bmatrix}\dot{u}_2 \tag{1b}$$

$$\dot{\sigma}_{12} = G\frac{1}{2h}\begin{bmatrix}1 & 1\\ -1 & -1\end{bmatrix}\dot{u}_1 + G\frac{1}{2h}\begin{bmatrix}-1 & 1\\ -1 & 1\end{bmatrix}\dot{u}_2 \tag{1c}$$

$$\dot{\sigma}_{a} = 2G\frac{1}{2h}\begin{bmatrix}1 & -1\\ -1 & 1\end{bmatrix}\dot{u}_1 \tag{1d}$$

$$\dot{\sigma}_{b} = 2G\frac{1}{2h}\begin{bmatrix}1 & -1\\ -1 & 1\end{bmatrix}\dot{u}_2 \tag{1e}$$

$$\ddot{u}_1 = \frac{1}{\rho}\frac{1}{2h}\begin{bmatrix}-1 & 1\\ -1 & 1\end{bmatrix}\sigma_{11} + \frac{1}{\rho}\frac{1}{2h}\begin{bmatrix}1 & 1\\ -1 & -1\end{bmatrix}\sigma_{12} + \frac{1}{\rho}\frac{1}{2h}\begin{bmatrix}-1 & 1\\ 1 & -1\end{bmatrix}\sigma_{a} \tag{2a}$$

$$\ddot{u}_2 = \frac{1}{\rho}\frac{1}{2h}\begin{bmatrix}-1 & 1\\ -1 & 1\end{bmatrix}\sigma_{12} + \frac{1}{\rho}\frac{1}{2h}\begin{bmatrix}1 & 1\\ -1 & -1\end{bmatrix}\sigma_{22} + \frac{1}{2h}\begin{bmatrix}-1 & 1\\ 1 & -1\end{bmatrix}\sigma_{b} \tag{2b}$$

Fig. 3. Two-dimensional velocity-stress finite difference scheme equivalent to the FLAC mixed discretization scheme for uniform elements. u_1 and u_2 are components of displacement, σ_{11}, σ_{22} and σ_{12} are components of stress, and dots indicate time derivatives. σ_a and σ_b are extra stress components which avoid hour-glassing. Large brackets denote the finite difference stencil. The scheme can readily be made fourth order accurate by including more distant terms (Hildyard, 2001)

scheme based on quadrilateral elements. It overcomes the problem of hour-glassing by subdividing the quadrilaterals into two overlayed sets of triangles, and using mixed discretization (Marti and Cundall, 1982), where a different discretization is used for the isotropic and the deviatoric components of stress and strain. Compared to the staggered grid, the approach is inefficient in both memory and run-time, and is only second order accurate which is inefficient for wave propagation problems. It was shown that this scheme can be reduced to an equivalent but significantly more memory efficient second order velocity-displacement scheme. It was also shown that for constant-sized elements, the mixed-discretization scheme can be reformulated into a scheme more similar to the staggered grid scheme, by the addition of two new grid variables (termed σ_a and σ_b). The scheme is illustrated in Fig. 3. The scheme was extended to form higher order finite difference schemes, with comparable memory and run-time efficiency to that of the higher order staggered mesh. Compared to the staggered mesh though, it holds the different components of stress at the same point in space, giving it advantages for more general studies of fractures. The method could significantly increase the efficiency in codes using the FLAC scheme, particularly in regions of uniform elements. The result is promising but requires extension to three-dimensions to be truly useful for modelling wave propagation.

The investigations covered above were not directly used in models in the following sections. However, they give a framework as to how such modelling can be extended in the future to include more complex patterns of fracture.

3. Comparison of models with laboratory experiments on seismic wave propagation through fractures

As noted in the introduction, two approaches have been pursued for representing seismic wave interaction with fractured rock, either encapsulating the behaviour of fractured rock through an effective elastic medium, or modelling fractures or groups of fractures explicitly. A displacement discontinuity is an explicit model, where the displacements on two surfaces of a zero-thickness interface are discontinuous, and the discontinuity in displacement is coupled to the surface stresses by a fracture stiffness. This fracture stiffness accounts for the existence of asperities and voids between the surfaces of natural fractures. A displacement discontinuity is widely used in rock mechanics for studying static behaviour. In these cases the two surfaces are often tightly coupled. For example, the approach in the code DIGS (Napier and Hildyard, 1992) corresponds to infinite fracture stiffness, where no relative displacement occurs unless there is failure (frictional sliding or tensile opening). The displacement discontinuity model of a fracture has also been studied for seismic wave propagation (Schoenberg, 1980; Myer et al., 1985, 1995). In this case the fracture stiffness has been shown to have a significant effect on wave propagation. The model has been shown to be consistent with experiments of recorded wave propagation through natural fractures in rock (Pyrak-Nolte et al., 1990a), in particular accounting for frequency-dependence of both the wave-speed and the amplitude. Researchers have also developed expressions for transmission and reflection coefficients based on different assumptions about coupling of the surfaces of the displacement discontinuity model.

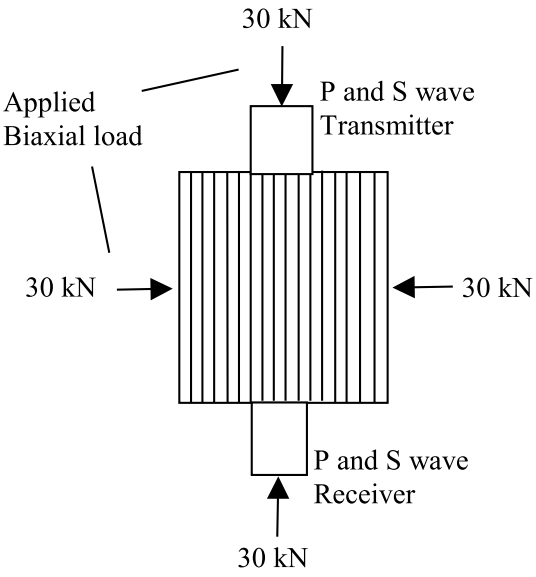

Fig. 4. Sketch of laboratory experiment on multiple fractures (Pyrak-Nolte et al., 1990b) showing the experimental system of packed steel plates, transmitter and receiver transducers, and bi-axial loading

Accurate modelling of wave propagation in the fracture zone requires that the wave behaviour is accurate for a considerable number of fractures and for the entire duration of oscillation. Consequently, the emphasis in this section was to accurately reproduce full waveforms for experimental data involving multiple fractures. The selected experiments were for wave propagation through a series of stacked steel plates (Pyrak-Nolte et al., 1990b). These experiments extended earlier results on single natural fractures (Pyrak-Nolte et al., 1990a). In the experiment, 31 mild steel plates were sandblasted to simulate fracture surfaces, and bolted to form a cube of side 90 mm (Fig. 4). The block was biaxially loaded at 30 kN, one load clamping the plates and a second parallel to the plates. P- and S-wave transmission was recorded for different orientations of the layered block and also for a solid steel cylinder to provide a control.

The experiment was modelled in three dimensions using 0.75 and 5.5 million fourth order accurate finite difference zones for the P- and S-wave models, respectively. The fractures were modelled using zero-thickness displacement discontinuities. Source waveforms for the P- and S-wave experiments were inverted from the waveform through the solid steel cylinder using Fourier transforms and applying the formula:

$$I_{\mathrm{Exp}}(\omega) = \frac{O_{\mathrm{Exp}}(\omega)}{O_{\mathrm{Tst}}(\omega)} I_{\mathrm{Tst}}(\omega) \tag{2}$$

where I_{Exp} is the inverted source waveform, O_{Exp} is the observed experimental response for solid steel, I_{Tst} is an arbitrary broad frequency test pulse and O_{Tst} is the response in the model of the solid cylinder to the test pulse. These inverted sources were then applied when modelling the fracture cases. Three simulations were made for P-wave propagation – the solid cylinder, horizontal fractures with wave propaga-

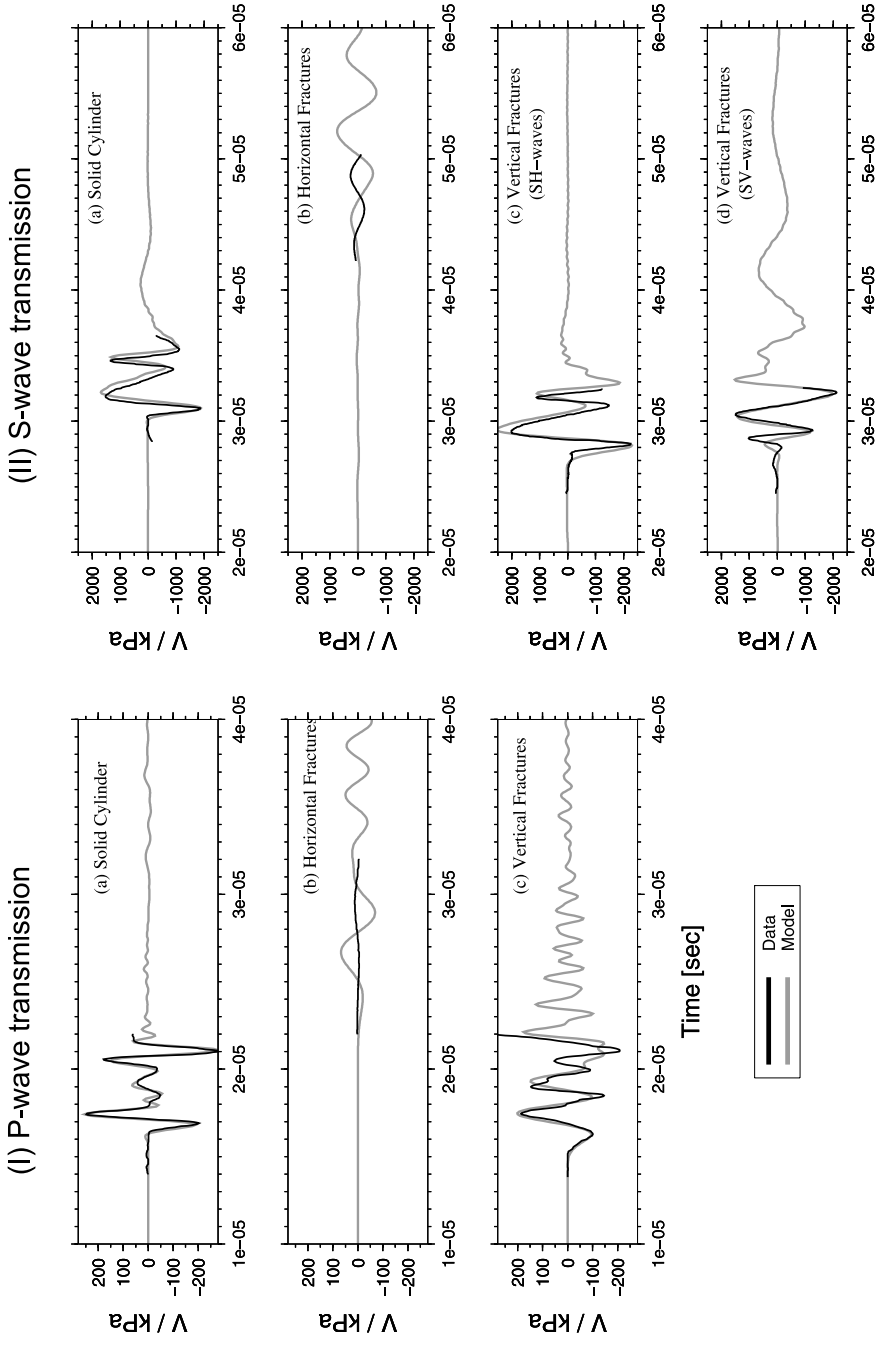

Fig. 5. Comparisons between experimental (Pyrak-Nolte et al., 1990b) and modelled seismograms for P- and S- waves transmitted through different orientations of multiple aligned fractures

tion across the fractures, and vertical fractures with wave propagation parallel to the fractures. Four simulations were made for S-wave propagation – the solid cylinder, horizontal fractures with wave propagation across the fractures, and two different polarisations for vertical fractures with wave propagation parallel to the fractures. In the first polarisation the excitation is parallel to the fractures (SH), while in the second the excitation is transverse to the fractures (SV). Initial models used a uniform normal and shear fracture stiffness of 6×10^{13} Pa/m and 2×10^{13} Pa/m, respectively, based on analysis from the original experiment.

The modelled and recorded waveforms are compared in Fig. 5. In each case the solid model matches the experiment, as is expected from the source inversion. Both P- and S-wave propagation across the fractures (Fig. 5, Ib and IIb) are significantly delayed, and attenuated, with a lower dominant frequency than the solid cases. Similar effects, with delayed arrival and reduced amplitude and frequency, are observed in the model, but to a much lesser degree than in the experiment. In all cases for propagation parallel to the fractures (Fig. 5, Ic, IIc and IId), the modelled waveforms are very similar to the observed waveforms. The effects on arrival and amplitude are not as severe as for wave propagation across the fractures, but the waveforms are significantly altered by the fractures and these changes are accurately predicted by the model. The thesis further compares the different cases in terms of the time-domain and frequency effects on waveforms and the effects on wave propagation patterns.

Overall there is a striking correspondence between the modelled waveforms and the recorded waveforms. This is primarily true for all cases of wave propagation parallel to the fractures. The modelled wave propagation across the fractures show similar effects on the arrival, amplitude and frequency to that observed in the experiment, but the model grossly underestimates the degree of attenuation and arrival delay. Variations were made to the fracture stiffness values to determine if improvements could be made for wave propagation across the fractures. Improved estimates of $K_n = 4.5 \times {}^{13}$ Pa/m, and $K_s = 2.5 \times 10^{13}$ Pa/m were obtained, but improvements were not significant. It was concluded that the arrivals and amplitudes could not be more consistently matched with a uniform value of fracture stiffness. However, the variations produced a very important result. The P-wave amplitude is significantly dependent on the shear fracture stiffness, which is not predicted by the theory for normal incidence on a single fracture. The influence is negligible for small numbers of fractures, but increases rapidly with increasing numbers of fractures, implying that this behaviour is due to multiple reflections.

The discrepancy in waveforms for propagation across the fractures leaves some doubt whether the displacement discontinuity model captures enough of the physics of a fracture, and whether it is suitable for representing wave propagation in the fracture zone. The differences in wave amplitude could indicate an additional dissipative mechanism in the fracture which removes mechanical energy from the system. This would be a fundamental alteration to the displacement discontinuity model. However, it was realised that the loading conditions in the experiment were not uniform. Fracture stiffness is related to the compression of a fracture and varies with normal stress across a fracture. A non-uniform stress field implies that rather than a single uniform fracture stiffness, the fracture stiffness should vary for different fractures, and also across an individual fracture. A new model was implemented with a

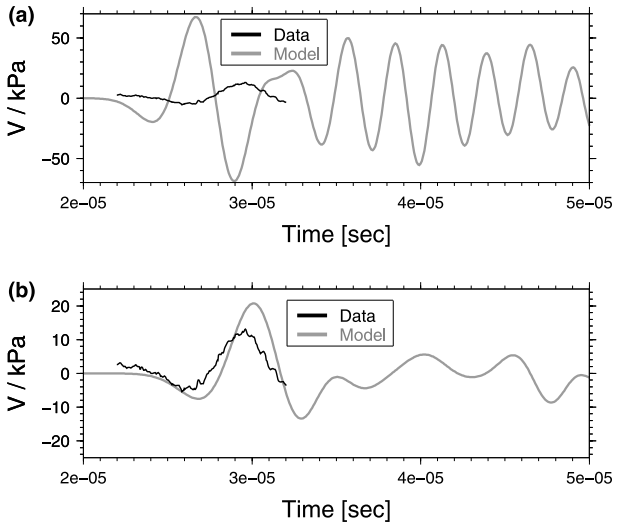

Fig. 6. Comparison of waveforms from the uniform stiffness model and the stress-dependent stiffness model, for horizontal fractures with P-wave propagation normal to the fractures (**a**) Uniform stiffness model (**b**) Stress-dependent stiffness model

stress-dependent fracture stiffness, based on a hyperbolic joint stiffness relation (Bandis et al., 1983).

Applying the non-uniform loading led to a non-uniform distribution in fracture stiffness, and was found to give greater attenuation and delay. Figure 6b shows that the waveform for P-wave propagation across the fractures, is now much closer to that of the data, matching the amplitude and arrival. The S-wave improvement was less convincing, but the overall effect was similar. The reason for the reduction in amplitudes in the stress-dependent model is apparent from the patterns of wave propagation (Fig. 7). The uniform fracture stiffness model (Fig. 7a) has wave-fronts which remain coherent across the whole block. Waves in the stress-dependent fracture stiffness model (Fig. 7b) propagate faster and more strongly through the centre of the model, leading ultimately to greater scattering of the wave. This indicates that the non-uniform loading leads to a non-uniform distribution in fracture stiffness, and can account for lower amplitudes without introducing a radical change to the displacement discontinuity model.

This section has shown that modelling wave interaction with displacement discontinuities captures much of the physics observed in experiments. A relatively simple model of a fracture convincingly matched the results of an experiment with many fractures. The work highlights the importance of fracture stiffness for modelling waves through fractures, as it has a significant effect on the waveforms, arrival, amplitude and frequency. Importantly, except in a completely uniform stress field, modelling wave propagation without considering the stress variation, is inaccurate. The stress-dependence of fractures can be accounted for with a stress-dependent fracture stiffness, and in a non-uniform stress field this stiffness may vary along a single continuous fracture. This has important consequences for modelling fractures around underground openings where stresses are highly non-uniform.

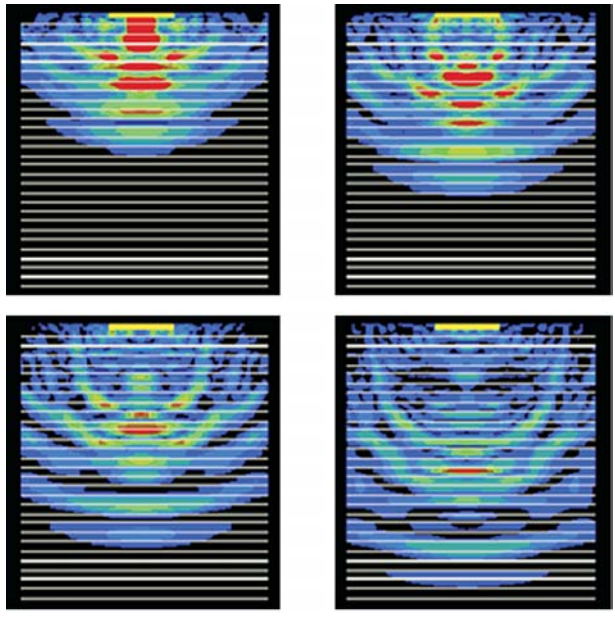

(a) Uniform fracture stiffness

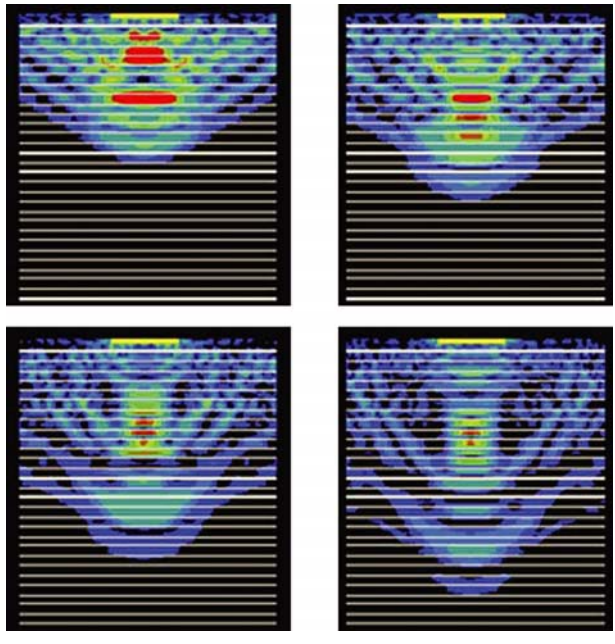

(b) Stress-dependent fracture stiffness

Fig. 7. Snapshots of particle velocity showing P-wave propagation through the horizontal crack model for (**a**) uniform stiffness cracks, and (**b**) stress-dependent stiffness cracks

4. Models of wave propagation through *in situ* fracturing around an underground excavation – a case study from the URL

A number of controlled *in situ* experiments have been made at the Underground Research Laboratory in Canada (URL). Ultrasonic velocity scans collected during an acoustic emission experiment at the URL (Carlson and Young, 1993), were used to extend the wave-fracture modelling to *in situ* fractures in rock at the surface of a deep tunnel. Their experiment monitored changes in a small volume of rock, approximately one cubic metre, near the face of an advancing tunnel. The velocity scans showed variations in both wave-speed and amplitude for different paths and interpretations were made on the fracturing.

The experiment was modelled in three-dimensions (Fig. 8), for a reduced 8×8 array of source-receiver combinations, and a model size of around 8 million zones. The tunnel surface was approximated as a flat free-surface. Initial models used an isotropic elastic medium, with the elastic wave-speeds of the intact rock. The ultrasonic sources were modelled by applying a velocity normal to the sensor orientation. Comparisons with the recorded waveforms showed many similarities such as the correct polarities for all P- and S- waves. However, all paths oblique to the tunnel surface were slower and of much lower amplitude than the elastic waveform. The full set of waveform comparisons with the source at sensor 3 are presented in Fig. 9. The elastic model identified that paths parallel to the tunnel surface are approximately elastic, while paths oblique to the tunnel surface are significantly lower than expected in both wave-speed and amplitude. Differences between the two path types were also evidenced in the frequency content of the waveforms. This indicates fractures aligned approximately parallel with the tunnel surface. Carlson and Young (1992) estimated the crack density to range between 0.12 and 0.09.

Two methods were used to investigate this fracturing. One conceptual model of fracturing is a collection of flat openings. A program was written to generate random crack assemblies with a specified crack density and a range of crack sizes. Crack

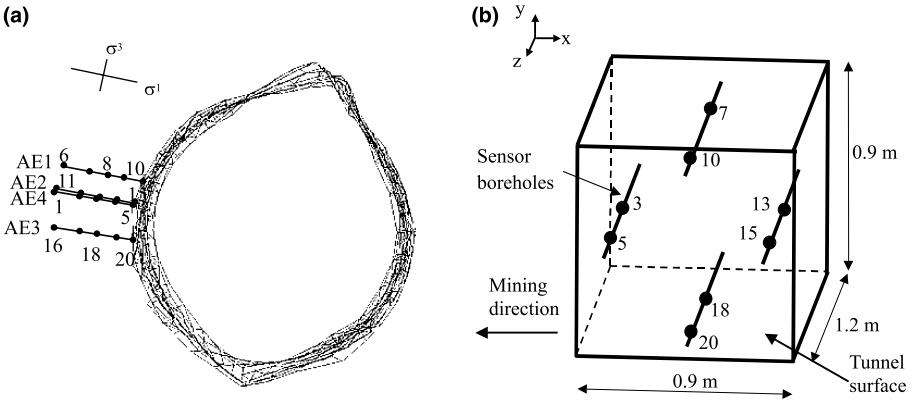

Fig. 8. Tunnel experiment. (**a**) Cross-sectional geometry of the acoustic array in the URL tunnel showing positions of boreholes AE1-AE4, and sensors 1–20. (**b**) Model geometry of a reduced 8×8 array, with boreholes rotated into a diamond pattern. The block indicates the model boundaries

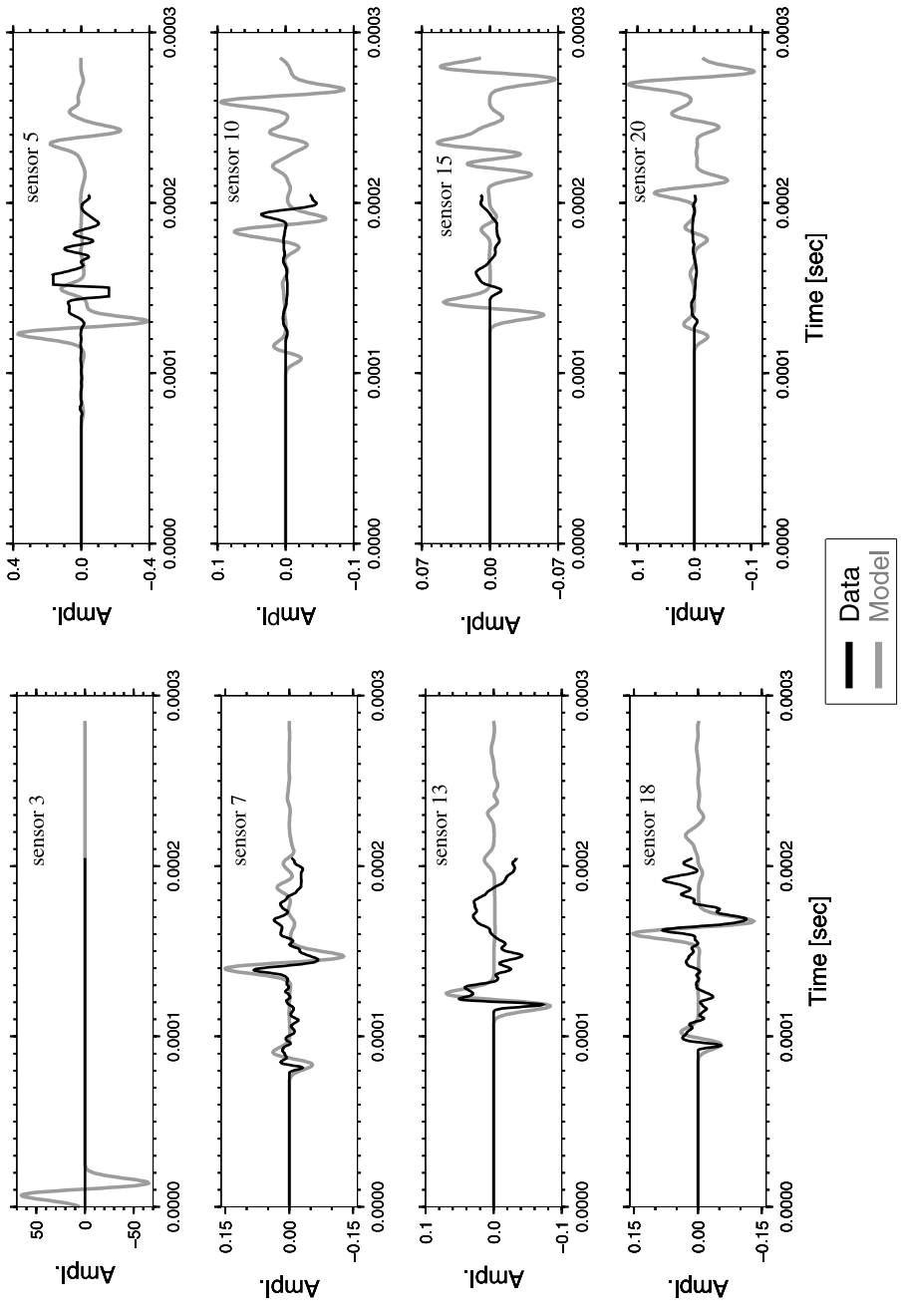

Fig. 9. Elastic model (grey line) compared to velocity scan AT01 (black line) for the source at sensor 3, and receiver sensors 3, 5, 7, 10, 13, 15, 18, 20. Paths on the left were approximately parallel to the tunnel surface while those on the right were oblique to the tunnel surface

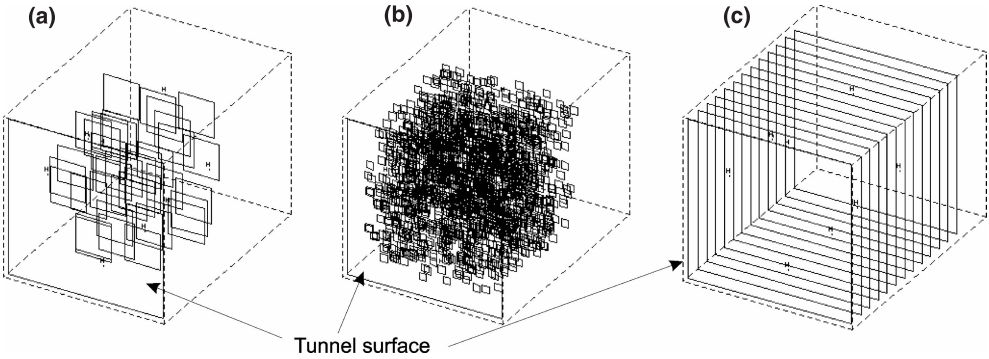

Fig. 10. Representation of fracturing in the tunnel models. (**a**) Crack assembly with crack density ($\varepsilon = 0.1$) comprising 38, 196.5 mm × 196.5 mm cracks (**b**) Crack assembly with crack density ($\varepsilon = 0.1$) comprising 6061, 36.5 mm × 36.5 mm cracks. (**c**) 12 large parallel stiff fractures with a spacing of 80 mm

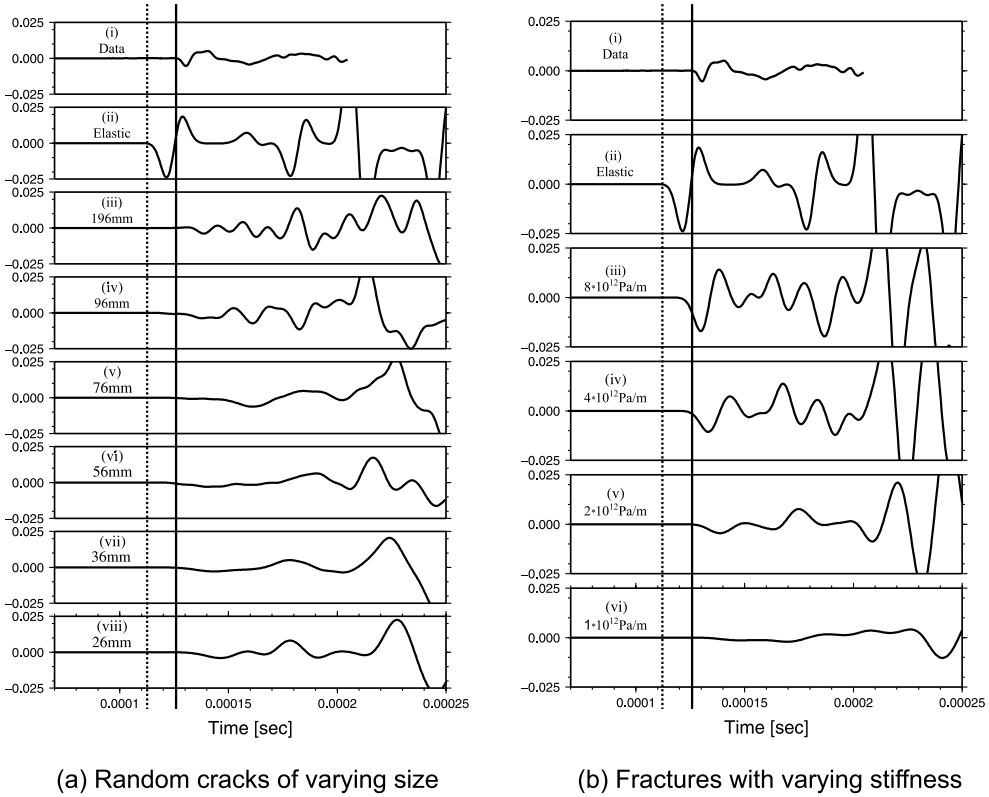

Fig. 11. Effect of fracturing on the waveform for a typical oblique path (path 3–20, cf. Fig. 9). (**a**) Comparison of waveforms for different crack assemblies with a constant average crack density of 0.1, and crack sizes ranging from 196 mm down to 26 mm. The dotted line indicates the P-arrival in the fully elastic model, and the solid line the P-arrival in the data. (**b**) Comparison of waveforms for large parallel cracks with a 80 mm spacing and fracture stiffness ranging from $8{*}10^{12}$ Pa/m down to $1{*}10^{12}$ Pa/m. The dotted line indicates the P-arrival in the fully elastic model, and the solid line the P-arrival in the data

density is a dimensionless quantity describing a collection of cracks (O'Connell and Budiansky, 1974). For circular cracks, crack density is proportional to the cube of the crack radius. For the rectangular cracks used in WAVE, crack density is given by

$$\varepsilon = \frac{1}{\pi V} \sum \frac{A^2 B^2}{A + B} \tag{3}$$

where A and B are the crack side-lengths, and V the volume of cracked region. A number of associated numerical issues were encountered with the method and these are examined in the thesis. Random crack assemblies of various sizes and crack density were introduced into the model of the experiment to examine their effect on the waveforms. Two examples are shown in Fig. 10a and b – these have equal crack density with a small number of large cracks, or a large number of small cracks. Figure 11a, shows how the waveform for one of the oblique paths alters for crack assemblies with the same average crack density, but with different sized cracks.

A second type of representation of the fracturing was to introduce large parallel fractures with fracture stiffness into the model of the experiment (Fig. 10c). Although more naturally applied as a model of a single fracture with contacts, this work explored whether it can be used to represent the effects of a collection of openings throughout a volume, rather than in a single plane. For it to be a useful technique, a relationship needs to be established between it and the underlying physical micro-crack configuration. Figure 11b, shows how the waveform for one of the oblique paths alters for a fixed fracture spacing, but with decreasing fracture stiffness.

Both methods of representing fracturing caused changes in the wave-speed and amplitude of waveforms, of the order of that observed in the data. The recorded behaviour was more consistent with models of smaller open fractures (26 mm) than with that of larger open fractures (196 mm), although practical numerical limits did not allow even smaller cracks to be investigated. The modelling confirms that the only single orientation of fractures consistent with the data for these paths, are fractures approximately parallel to the surface. The modelling also suggests that the crack density was over-estimated in the original analysis. Such modelling could benefit acquisition systems, testing the consistency of conclusions from the data analysis, in particular conclusions on the density, orientation and size of fracturing.

A qualitative study on the effects of fracture spacing and fracture stiffness indicated that the fracture stiffness had the greatest influence on the amplitude, while decreasing either the fracture stiffness or spacing, decreased the wave-speed. In a rough sense, the fracture stiffness may be related to the sizes of openings, while both fracture stiffness and spacing relate to the crack density. The representation using stiff fractures does not suffer from the numerical resolution difficulties associated with the attempts to represent the true size of crack openings, and could therefore be a useful model of effective fracturing for matching the wave behaviour for large scale models. A link then needs to be established between the effective representation and the underlying assembly of micro-cracks.

Motivated by the above, a method was developed to characterize the frequency dependence of both wave-speed and amplitude in fracture models. This was used to under-

stand the effects of crack density and crack size. It explains why models of the experiment with different crack sizes but equal crack densities had different effects on arrival time and amplitude. It also provides a method by which a relationship can be established between models with larger stiff fractures and accumulations of smaller open cracks. A large body of research has focussed on these issues including analytical, experimental and more recently numerical studies. These include developing analytical expressions for wave-speed and attenuation due to fracture assemblies, studying wave propagation through single and multiple aligned stiff fractures, and the relationship of fracture stiffness to areas of contact and opening. Using a numerical approach as outlined here offers certain benefits over these studies. Expressions are obtained for both attenuation and phase velocity, and these are directly obtained as a function of frequency. The expressions are not limited to wavelengths much larger than the fracture sizes and the analysis is not necessarily limited to the study of plane waves. Finally, most of the cases necessarily require a three-dimensional treatment, which has not been attempted in other numerical studies.

The method used is to approximate plane wave propagation through a three-dimensional model containing fractures. A recording (waveform-2) is made at the end of the fractured region and compared against the waveform from a perfectly elastic medium recorded at the start position of the fractured region (waveform-1). Using Fourier Transforms of the waveforms, phase velocity (c) and attenuation (A) can be calculated as a function of frequency (ω) from

$$c(\omega) = \omega|x_2 - x_1| \left[\frac{-(\phi_2 - \phi_1) - i \ln\left(\frac{A_2}{A_1}\right)}{(\phi_2 - \phi_1)^2 + \left[\ln\left(\frac{A_2}{A_1}\right)\right]^2} \right] \tag{4}$$

$$A(\omega) = \left(\frac{A_2}{A_1}\right)^{\frac{L}{|x_2 - x_1|}} \tag{5}$$

where $A_1(\omega)$ and $A_2(\omega)$ are the Fourier amplitude functions and $\phi_1(\omega)$ and $\phi_2(\omega)$ the Fourier phase functions of the elastic and recorded waveforms respectively, x_1 and x_2 are the positions of the recorded waveforms and L is the unit distance of interest. It is also possible to calculate $Q(\omega)$ from the attenuation function and the phase velocity.

$$Q(\omega) = \frac{\pi \frac{\omega}{c(\omega)} x}{\ln\left(\frac{A_2}{A_1}\right)} \tag{6}$$

The procedure is demonstrated in Fig. 12 with the results shown in Fig. 13a. Significantly, the time domain waveforms do not necessarily show a clear difference in arrival time (Fig. 12b). This is due to the high frequencies contained in the source, which are attenuated but not slowed for this crack-size. In contrast, the phase difference (Fig. 12d) and the calculated phase velocity (Fig. 13a) clearly indicate a reduction in velocity for the low frequency region. The results for phase velocity calculations were found to be consistent and repeatable, but sensitive to certain numerical issues, primarily related to practical limits on the model size. The models were (for that point in time) at the limit of capability with approximately 12 million grid-points.

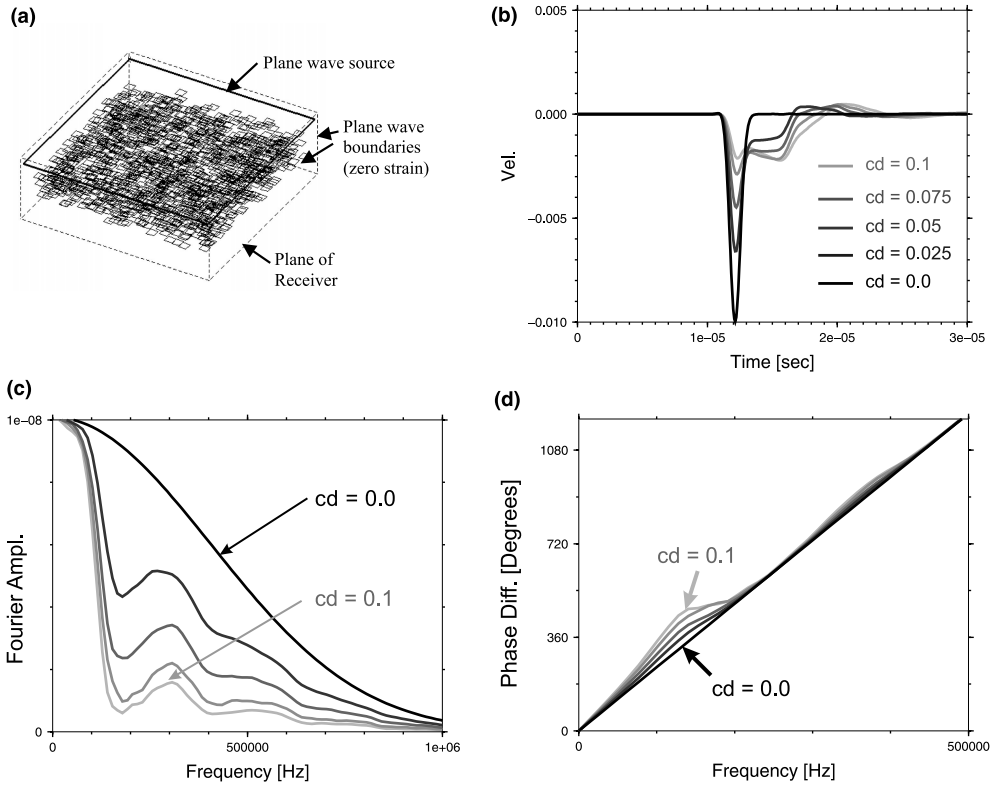

Fig. 12. Stages for calculating phase velocity and attenuation spectra in crack models. (**a**) Simulated fracture medium (**b**) Time domain waveforms for the crack models (**c**) Fourier amplitude spectrum (**d**) Phase spectrum difference between emerging and input waveforms. Models have 11.3 mm cracks with 296, 591, 887 and 1182 cracks, respectively, corresponding to crack densities of 0.025, 0.050, 0.075 and 0.1, and are compared to an uncracked model (black). The resulting phase velocity and attenuation functions are shown in Fig. 8a.

A wide range of fracture sets were studied using this method, including random distributions of a large number of small open cracks of varying size and crack density, and larger fractures with surfaces coupled by a fracture stiffness. Some typical results are shown in Fig. 13. The curves indicate that wave-speed is not constant with frequency. It decreases from its low frequency value by another 30–50%, and then increases back toward the elastic wave-speed such that high frequencies are attenuated but not slowed. Increasing crack density leads to successive decreases in the low frequency phase-velocity. Studies also showed that an increase in fracture stiffness increases the phase velocity and shifts the frequency at which high attenuation occurs to a higher frequency, a change consistent with that of a lower crack density and smaller open cracks. The work has important implications for seismic interpretation in that wave-speeds measured in the time-domain cannot be used to uniquely determine crack density. This seems to be a useful quantitative approach for numerically investigating the effects of fractures, and could be extended to study a wide range of fracture types and assemblies.

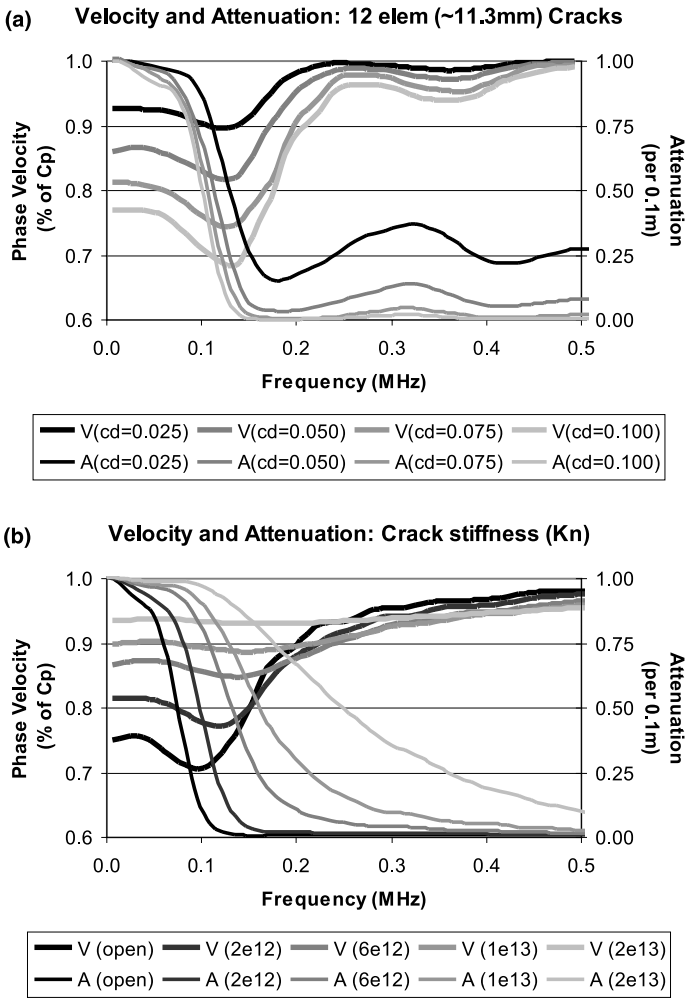

Fig. 13. Phase velocity (V) and attenuation (A) spectra for crack distributions. (**a**) Distribution of 11.3 mm open cracks with a crack density of 0.025, 0.05, 0.075 and 0.1. (**b**) Distribution with crack lengths ranging from 7.3 to 19.3 mm, a crack density of 0.1, and varying fracture stiffness

5. Evaluating the influence of an excavation on the distribution and amplitudes of ground motion

The previous sections indicate some success in duplicating the behaviour of measured wave propagation through fractures. There were two motivations for this work. The potential to aid the interpretation of fracturing around excavations has been demonstrated. The second application is to improve the forward modelling of wave propagation around excavations. This section returns to the rockburst problem discussed in the introduction, and considers the effect of the excavation and fracturing on the ground motions in excavations.

Understanding the maximum ground motions due to a rockburst, its decay, and the regions of large ground motion, has important consequences for hazard analysis and support design. However, a number of questions remain unanswered in the field of rockburst study. What are the maximum in-stope amplitudes caused by a seismic event (McGarr, 1993; Ortlepp, 1993; Spottiswoode et al., 1997)? What mechanisms lead to motions in stopes being much larger than those in the solid rock (Hemp and Goldbach, 1993; Milev et al., 1999)? What affects the observed distribution of damage and why does damage sometimes occur at large distances from the original event (Durrheim et al., 1997)? This section uses models to evaluate the effect of the excavation on ground velocity and in so doing attempts to address these questions. It first evaluates the influence of the stope's free surface alone and highlights certain features of Rayleigh waves. It then examines the effect of variations in the geometry and source on the amplitude of ground motion. Different representations of the fracture zone are introduced to determine whether this indeed leads to amplification. Finally, it considers the potential for triggered energy release to cause increased ground motions.

A mining problem is used throughout this section to examine the effects of an excavation on wave propagation. It consists of a tabular stoping geometry typical of long-wall mining in deep-level mines in South Africa. Figure 14a shows a plan view of the mining layout with the mining direction towards the right. The mining layout

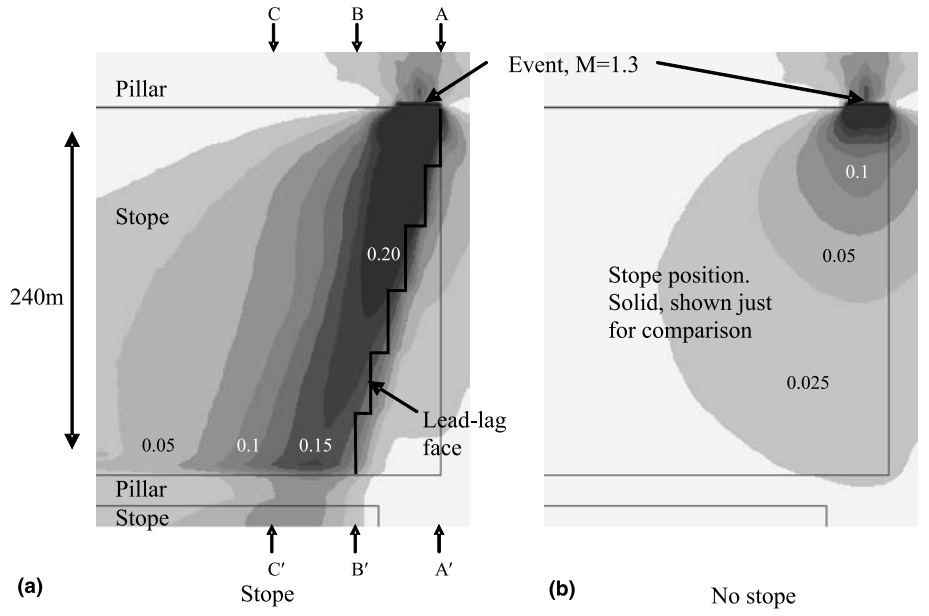

Fig. 14. The projected influence of a mining layout on the wave propagation from a seismic event. Plan sections are shown through two three-dimensional elastic models. Model (**a**) contains a tabular mining excavation, while model (**b**) has a purely solid material. Contours indicate the maximum vertical velocity (in m/s) induced in a plane just below the excavation by a particular seismic event of magnitude 1.3. The event occurred in the foot-wall of the pillar, parallel to the direction of mining advance, just behind the face position of the mining. The influence of the stope on the wave propagation causes velocities at a far pillar to be up to six times that of the solid model without the excavation

consists of the stope, which is a narrow excavation of 1.5 m height extending for hundreds of metres, and pillars, which are solid regions left for stability reasons. The 'stepped' outline shows the mining face position or lead-lag face. The pillars are highly stressed and hence can be the source of seismicity. Wave propagation was simulated for a vertical slip event in the foot-wall of the pillar. The region of slip was 28 m by 28 m, with source centre 2 m into the pillar, 12 m below the stope, and 12 m back from the stope face (Fig. 14a). The rupture was propagated at 3000 m/s, with a uniform stress drop of 9.35 MPa. The stress drop at any point occurred over 2 ms, and the whole event over 6 ms. The event had a moment of $1.2*10^5$ MNm, and a moment magnitude of 1.3.

Figure 14 compares the maximum vertical velocity in a plane 2 m below the stope with the case if the excavation did not exist. The excavation significantly influences both the amplitude and the distribution of the largest motions. Maximum amplitudes follow the face outline, and the maximum amplitudes deep into the stope are around four times those at similar distances in the solid model. An even more marked effect is observed in the induced tensile stresses, where the value 200 m from the event is increased from 0.06 MPa in the solid model to 1.6 MPa due to the influence of the excavation. Figure 15 indicates that the distribution of tensile stress at the surface is very similar to that of the maximum velocity, but decays sharply with distance from the free surface. It is hypothesised that this induced stress may be significant in triggering energy release in the low stress, failed regions of the stope hanging-wall and foot-wall, or in the highly stressed regions of the pillars.

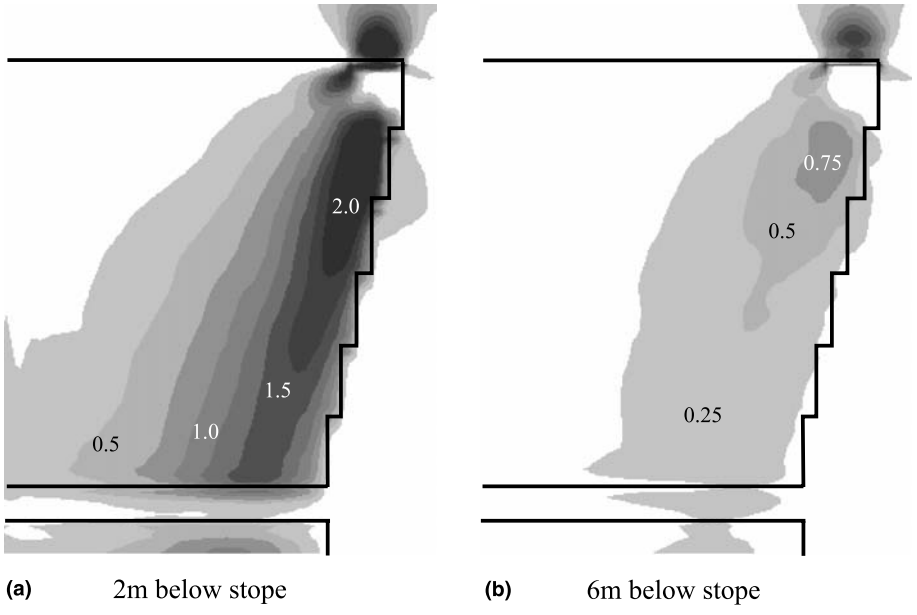

Fig. 15. Maximum induced tensile stress (in MPa) for σ_{zz}. Plan sections are shown for two distances below the excavation, and indicate that horizontal tensile stress of up to 2 MPa is induced close to the surface, and that this falls off rapidly with distance from the surface

It is significant that just a 1.3 magnitude event near the edge of a stope can lead to these motions and induced tension 200 m from the event. This is caused by surface waves propagating along the free surface of the stope, although for these wavelengths and distances the shear and Rayleigh waves do not separate, and motion is made up of both body and surface waves. A study was made of Rayleigh waves propagating along the hanging-wall of an infinite stope. Figure 16 compares the decay in velocity and tensile stress for two different sources with peak frequencies of 330 Hz and 120 Hz.

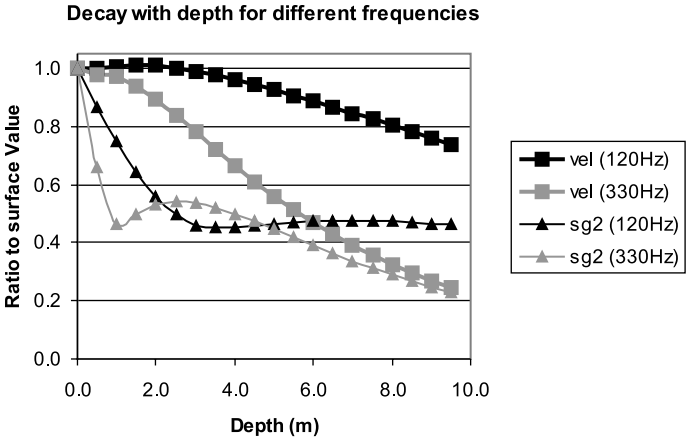

Fig. 16. Decay with depth from the stope surface for velocity and maximum tensile stress for different frequencies. (**a**) Peak frequency of 330 Hz ($\lambda \approx 10$ m) (**b**) Peak frequency of 120 Hz ($\lambda \approx 27$ m)

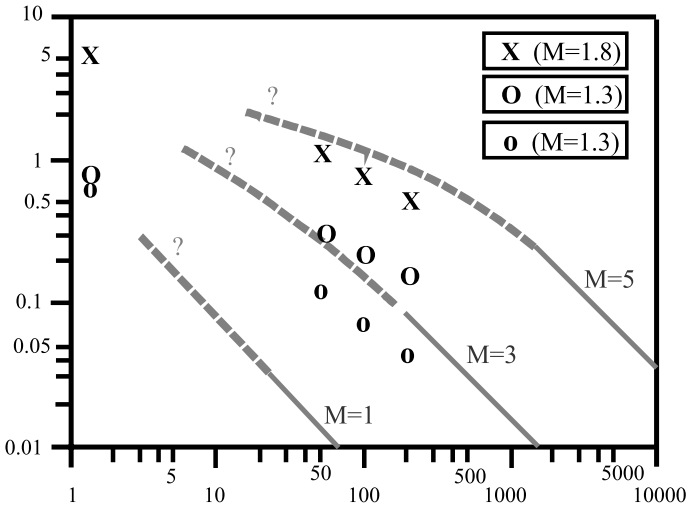

Fig. 17. Far-field and projected near-field velocities for different magnitude events (from Jager and Ryder, 1999), with velocities for three of the modelled events superimposed on the original graph (shown as "o", "O" and "X"). The presence of the stope, and events with a high stress-drop, lead to in-stope velocities associated with much larger magnitude events

For small, high frequency events, the decay is rapid, and velocity at the surface is many times more than that a few metres into the solid. Measurements have been made where particle velocities were many times higher at the surface than a few metres into the fracture zone (e.g. Milev et al., 1999), and this has been interpreted as amplification due to the fractured rock. The above analysis shows that some of the apparent amplification may be explained by Rayleigh waves rather than by the effect of the fracture zone.

The layout of Fig. 14 was further analysed to determine the effect of variations in the source, such as higher stress-drops, orientation of slip and proximity of source to stope (including intersection with the stope, termed 'daylighting'), on peak velocities. The peak near-source velocities were up to 70% higher than upper limits commonly estimated using the formula ($V_{max} \approx 1.1\tau_e/(G\beta)$) (Jager and Ryder, 1999). Figure 17 shows a graph from Jager and Ryder (1999) of far-field velocities and estimates of near-field velocities for different magnitude events, with values from three of the modelled events superimposed. The two modelled events which include the excavation, have much higher velocities, and decay more slowly than that projected by Jager and Ryder. The presence of the stope therefore leads to in-stope velocities normally associated with much larger magnitude events.

The hanging-wall and foot-wall of deep-level mining stopes are highly fractured due to stress-induced fracturing and natural discontinuities. Fractures cause waves to attenuate due to scattering of high frequencies, but also reduce the effective elastic modulus of rock, which may increase amplitudes for long wavelengths. The effect of fractures on the peak near-field and far-field velocities was therefore evaluated for stope-normal (vertical) and stope-parallel (horizontal) fractures. Figure 18 shows two cases for vertical fracturing with crack densities of 0.01 and 0.1. Table 1 summarises the results from some of the fracture models, by comparing the peak near-field and far-field velocities and induced tensile stresses to that of an unfractured model. Vertical fractures had no effect on the near-field amplitudes, but horizontal fracturing increased the peak near-field velocities (by up to 50% for some models). Both orientations of fractures accounted for increased amplitudes at more distant parts of a stope. The amplitudes decrease if the fracture stiffness is low, which may indicate that the propagation of surface waves is inhibited by very open fractures.

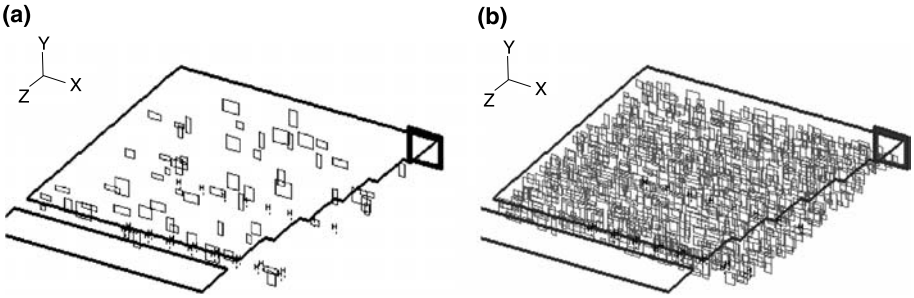

Fig. 18. Stope model with vertical fractures in the foot-wall of the stope. The fractures are rectangular with edge-lengths between 4 m and 14 m, and are in a band between 4 m and 18 m below the stope. (**a**) Fracture density of 0.01 (**b**) Fracture density of 0.1

Table 1. Ratio of maximum in-stope velocity and maximum induced tensile stress at 40 m and 200 m from the event, for different models of the fracture zone compared to the unfractured model

Model	Fracture stiffness		Max. at 40 m		Max. at 200 m	
	Normal (Pa/m)	Shear (Pa/m)	Velocity	Tensile stress	Velocity	Tensile stress
E: Horizontal fractures (extensive and parallel)						
E1	1×10^{16}	1×10^{11}	1.00	1.00	1.18	1.03
E2	4×10^{10}	2×10^{10}	1.19	1.07	1.21	1.03
E3	1×10^{10}	5×10^{9}	1.50	1.11	1.12	0.63
F: Horizontal fractures (finite and random)						
F1	1×10^{10}	5×10^{9}	1.16	1.07	1.45	0.94
G: Vertical fractures (finite and random)						
G1	1×10^{16}	1×10^{11}	1.00	1.00	1.09	1.03
G2	4×10^{10}	2×10^{10}	1.00	1.00	1.10	1.00
G3	1×10^{10}	5×10^{9}	1.00	0.96	1.09	0.88
G4	1×10^{10}	5×10^{9}	1.00	0.96	1.24	0.88

Values are given in absolute terms and as a ratio to that of the unfractured model. Models of type (E) contained horizontal fractures parallel to the stope and extending across the same area as the stope. Models of type (F) contained smaller random horizontal fractures. Models of type (G) contained random vertical fractures.

The fracturing also affects the distribution of maximum velocity and the nature of the waveforms.

Although the models showed that even small magnitude events can account for maximum velocities of more than 1 m/s, much larger velocities have been inferred in observations of failed rock (Ortlepp, 1993). One explanation for large velocities is that the waves may trigger failure in a highly stressed region (e.g. within a buckling slab, McGarr, 1997). Another model proposed by Linkov and Durrheim (1998), is amplification due to additional energy release as waves pass through the fracture zone which is in a post-failure, strain-softening state. A related mechanism was investigated by assuming residual stresses on the fractures and investigating whether waves from the event would cause additional energy release and whether this would increase the amplitude of the wave motions. The results were that some failure took place on all fractures, generating source magnitudes on individual fractures ranging from -2.5 to 0.35, and a total moment of 6.10^5 MNm – five times that of the original event. Nevertheless, the distribution of maximum velocity was no larger than the original event, and motions were smaller than that obtained with soft, linear fractures. There were, however, pockets of high velocity associated with triggered events in areas where there was previously low ground motion, and seismograms were also considerably altered. The conclusion is that although considerable energy release occurs, this is not coherent and does not lead to the amplification of the original wave, but rather manifests itself in localised pockets of large motions, sometimes in unexpected areas.

A more detailed account is given in Hildyard et al. (2001). This work has shown that the amplitudes in both the near- and far- field are complexly influenced by the following: stress drop, sense of slip, excavation surface, excavation outline, and the proximity of any part of the source, rather than the source centre, to the excavation. In

these models, the stope free-surface caused up to a 40% increase in near-field and up to a 600% increase in far-field velocities, while fracturing caused up to a 50% increase for both near- and far-field stope velocities. The conclusion is that the damage potential from an event near an excavation cannot be readily inferred from aspects such as moment, magnitude and the proximity to the source centre, as this ignores the effect of free surfaces and fracturing.

6. Conclusions

The work summarised here, contributes to science and technology through an improved understanding of wave propagation through fractured rock and the increased ability to simulate such behaviour. It has capacity for real world application in engineering fields such as mining, underground waste depositories and oil exploitation.

(i) Representation of fracturing

Complex three-dimensional wave behaviour has been realistically modelled using a mechanistic model of fracture, specifically a displacement discontinuity. Although based on theoretical models developed some years ago, this is possibly the first numerical demonstration that a mechanistic model of fracturing can accurately reproduce significant changes in waveforms in non- plane-wave propagation through multiple fractures. The fracture stiffness significantly affects the waveforms, arrival delay, amplitude and frequency content, and the degree of attenuation of high frequencies and amplification of lower frequencies. The shear fracture stiffness was shown to influence the amplitude of first arrivals for P-wave transmission through multiple fractures – a result not predicted by the theory for a single fracture. The importance of stress-dependence on the fracture stiffness was also established. A model with stress-dependent fracture stiffness was investigated and the stress state significantly affected wave propagation. It is not sufficient to simply allow opening of fractures in tension, as significant differences in wave propagation occur even when all fractures are in compression.

Two explicit models of fracturing were used in modelling *in situ* experiments – large fractures with fracture stiffness and accumulations of small open cracks. Both accounted for observed effects on wave-speed and amplitude, for waves across fractures and for waves parallel to fractures. However, it may be impractical to model the true openings in the material to account for waveform changes in *in situ* monitoring. The wave propagation changes on a larger-scale could then more readily be accounted for by using a distribution of stiff rather than open fractures. Understanding the underlying crack openings, for example for fluid flow, could then use smaller-scale wave models to investigate how the effective fractures relate to the underlying physical state.

With the above in mind, a numerical technique was developed to characterise the wave behaviour for various models of fracturing across a wide frequency band. Using this numerical technique should have advantages over theoretical analyses, as less restrictive cases can be studied and since it can be readily applied to investigate new, alternative or more complex models of fracturing. The method involves simulating plane wave propagation through an assembly of fractures and then ex-

tracting the frequency variation in phase velocity and attenuation from the resulting waveforms. Phase velocity and attenuation spectra were calculated for various sizes and densities of open fractures, as well as for large fractures with varying fracture stiffness and fracture spacing. These results should be useful in their own right, but the technique could be readily applied to study a much wider range of fracture models and has the capacity to provide greater insight to interpretations of fracturing from seismic recordings.

(ii) Capacity for real world application

Two main applications have motivated this work. The first is forward-modelling to project the wave propagation around underground openings. Reliable simulation of wave propagation would have important benefits for hazard analysis, since understanding the amplitude and distribution of ground motions is the first step in anticipating regions of likely damage due to seismic events. This goal has been advanced by modelling case studies where the wave behaviour was shown to correspond to observed behaviour, albeit in highly-controlled experimental conditions.

The second application is to aid the analysis of recorded data to interpret the fractured state of rock. This is important to the fields of mining, oil extraction and nuclear waste storage. Models allow the interpretation to go beyond average seismic properties of rock (wave-speeds and attenuation) and to help interpret the underlying structure of fracturing and stress-state, giving a physical basis for the wave-speeds and attenuation derived by seismic analysis. Models also allow conclusions on the density, orientation, size of fractures, and the stress state, to be verified. The potential for this has been established through the modelling of the URL data, where insight was given into the crack density and the size of open cracks.

The results on fracture stiffness have important consequences for modelling waves around underground openings. Large fractures must not be considered as simply open or closed. The stress distribution around underground excavations is extremely non-uniform and the stress-dependence of the fracture stiffness is therefore also important when simulating wave propagation around these openings. The dependence of fracturing on stress state indicates that projecting the wave propagation around openings is ultimately a coupled problem of solving the *in situ* stress state together with the seismic loading.

The investigations indicate that coupling modelling with the measurement of seismic waveforms will aid in interpreting the rock mass condition. The modelled fracturing causes both wave-speed and amplitude changes and provides a method of verifying the consistency of conclusions acquired through seismic monitoring. It was found to be presently impractical to model the true crack openings in the material for *in situ* monitoring. A two-phase approach was proposed, where the true openings can be investigated in smaller-scale models. The approaches used for modelling the ultrasonic source and for inverting for the source will also be useful for future analyses of such data.

In rockbursts, the amplitudes of ground motion in both the near- and far- field were shown to be complexly influenced by stress drop, sense of slip, excavation surface, excavation outline, and the proximity of any part of the source, rather than the source centre, to the excavation. Fractures influenced amplitudes in both the near-

source and far-field region. The amplification reported by researchers was investigated, and simulations showed that fracturing and the excavation itself can provide explanations on this apparent amplification. The damage potential from an event near an excavation cannot be simply inferred from aspects such as moment, magnitude and the proximity to the source centre, as this ignores the effect of the excavation and fracturing, i.e. simulations will be required for meaningful estimates of damage potential.

(iii) Numerical contributions

A number of numerical contributions have been made which are important for models of wave propagation around underground openings. It was shown that a finite difference approach could be used to study wave interaction with very large numbers of fractures (tens of thousands in some models). A numerical method was developed which allows the dispersion characteristics of a numerical code to be studied. The approach calculates the variation of phase or group velocity and amplitude with frequency, without any need to analyse the underlying method. This allowed the accuracy and efficiency of a number of codes to be examined and results support the need for specialised codes for studying wave propagation. A number of methods were investigated for generalising the staggered grid scheme to support angled cracks: a scheme based on a localised transversely isotropic material was found to be unsuitable; a second order approximation to an explicit angled crack was developed, but the method is not suited for modelling completely general fracture geometries; a scheme was derived for mapping the orthogonal grid to a curvilinear grid but the implementation of a crack requires derivatives which are not accurately approximated in the staggered mesh. A new finite difference scheme was developed which is fourth order accurate in space, does not exhibit hour-glassing, and has a memory and run-time efficiency comparable to that of the staggered mesh. The different components of stress are held at the same point in space, giving it an advantage over the staggered mesh for more general studies of fracturing, cavities or free surfaces. If this scheme could be extended to three-dimensions it would be a very attractive scheme for future wave and fracture studies.

Acknowledgements

Thanks are due to Paul Young who created a research environment that was both fun and stimulating, and for continued interaction and stimulation in subsequent years; to John Napier for many years of useful interaction and for initiating me in this line of research; to Peter Cundall who introduced me to finite difference techniques; to my employers at the time, CSIR in South Africa, for supporting the research; and to SIMRAC (Safety in Mines Advisory Council), who funded the projects under which this work was researched.

References

Aki K, Richards PG (1980) Quantitative seismology: theory and methods. Freeman, Cooper, San Francisco, vol. 2, section 13.6, pp 773–795

Bandis SC, Lumsden AC, Barton NR (1983) Fundamentals of rock joint deformation. Int J Rock Mech 20(6): 249–268

Brady BH (1990) Dynamic performance and design of underground excavations in jointed rock. In: Brummer RK (ed) Static and dynamic considerations in Rock Engineering. Balkema, pp 1–11

BSSA (1991) The 1989 Loma Prieta, California, earthquake and its effects: special issue. B Seismol Soc Am 81(5): 1415–2166

Carlson SR, Young RP (1992) Acoustic emission and ultrasonic velocity study of excavation-induced microcrack damage in the mine-by tunnel at the underground research laboratory. Report #RP015AECL to Atomic Energy of Canada, pp 1–50

Carlson SR, Young RP (1993) Acoustic emission and ultrasonic velocity study of excavation-induced microcrack damage at the underground research laboratory. Int J Rock Mech 30(7): 901–907

Coates RT, Schoenberg M (1995) Finite-difference modelling of faults and fractures. Geophysics 60(5): 1514–1526

Cook NGW (1992) Natural joints in rock: mechanical, hydraulic and seismic behaviour and properties under normal stress. Int J Rock Mech Min Sci Geomech Abstr 29: 198–223

Crampin S (1981) A review of wave motion in anisotropic and cracked elastic-media. Wave Motion 3: 343–391

Cundall PA (1992) Theoretical basis of the program WAVE. Unpublished internal report, COMRO (now CSIR, Division of Mining Technology, South Africa), pp 1–12

Cundall PA, Lemos JV (1990) Numerical simulation of fault instabilities with a continuously-yielding joint model. Proc. of 2nd Int. Symp. on Rockbursts and Seismicity in Mines. Balkema, pp 147–152

Daehnke A, Hildyard MW (1997) Dynamic fracture propagation due to stress waves interacting with stopes. Proc. of 1st Southern African Rock Engineering Symposium (SARES). Johannesburg, South Africa, pp 97–108

Daehnke A, Rossmanith HP, Knasmillner RE (1996) Using dynamic photoelasticity to evaluate the influence of parting planes on stress waves interacting with stopes. Int J Numer Anal Met 20(2): 101–117

Durrheim RJ, Roberts MKC, Hagan TO, Jager AJ, Handley MF, Spottiswoode SM, Ortlepp WD (1997) Factors influencing the severity of rockburst damage in Southern African gold mines. Proc. of 1st Southern African Rock Engineering Symposium (SARES). Johannesburg, South Africa, pp 17–24

Graves RW (1996) Simulating seismic wave propagation in 3D elastic media using staggered-grid finite differences. B Seismol Soc Am 86(4): 1091–1106

Handley MF, Hildyard MW, Spottiswoode SM (1996) The influence of deep mine stopes on seismic waves. Proc. of the 2nd North American Rock Mechanics Symposium (NARMS). Montreal, pp 499–506

Hemp DA, Goldbach OD (1993) The effect of backfill on ground motion in a stope. In: Young RP (ed) Proc. of 3rd Int. Symp. on Rockbursts and Seismicity in Mines. Balkema, pp 75–79

Hestholm S, Ruud B (1994) 2D finite-difference elastic-wave modeling including surface-topography. Geophys Prospect 42(5): 371–390

Hildyard MW (1995) WAVE developments. In: Develop a quantitative understanding of rock-mass behaviour near excavations in deep mines. Unpublished SIMRAC final project report (GAP029), December 1995. CSIR Mining Technology, Johannesburg, South Africa, pp 17–51

Hildyard MW (2001) Wave interaction with underground openings in fractured rock. PhD Thesis, University of Liverpool, pp 1–283

Hildyard MW, Milev AM (2001a) Simulated rockburst experiment: development of a numerical model for seismic wave propagation from the blast, and forward analysis. J South African Inst Min Metall 101(5): 235–245

Hildyard MW, Milev AM (2001b) Simulated rockburst experiment: numerical back-analysis of seismic wave interaction with the tunnel. J South African Inst Min Metall 101(5): 223–234

Hildyard MW, Young RP (2002) Modelling wave propagation around underground openings in fractured rock, Special issue on induced seismicity, ed., Trifu. Pure Appl Geophys 159: 247–276

Hildyard MW, Daehnke A, Cundall PA (1995) WAVE: a computer program for investigating elastodynamic issues in mining. Proc. of 35th US Symp. on Rock Mech, June 1995. Balkema, pp 519–524

Hildyard MW, Napier JAL, Young RP (2001) The influence of an excavation on ground motion. Proc. of 5th Symp. on Rockbursts and Seismicity in Mines (RaSiM 5). Johannesburg, Sept. 2001, SA Inst. Min. Metall., pp 443–452

Hudson JA (1981) Wave speeds and attenuation of elastic waves in material containing cracks. Geophys J Roy Astr S 64: 133–150

Itasca Consulting Group (1993a) UDEC Version 2.0. Minneapolis, Minnesota

Itasca Consulting Group (1993b) FLAC Version 3.2. Minneapolis, Minnesota, pp 1–20

Jager AJ, Ryder JA (1999) A handbook on rock engineering practice for tabular hard rock mines. Published by The Safety in Mines Research Advisory Committee (SIMRAC). Johannesburg, South Africa

Jiangfeng Z (1997) Quadrangle-grid velocity-stress finite-difference method for elastic wave propagation simulation. Geophys J Int 131: 127–134

Linkov AM, Durrheim RJ (1998) Velocity amplification considered as a phenomenon of elastic energy release due to softening. Mechanics of Jointed and Faulted Rock, Balkema, pp 243–248

Liu ER, Hudson JA, Pointer T (2000) Equivalent medium representation of fractured rock. J Geophys Res 105(B2): 2981–3000

Mack MG, Crouch SL (1990) A dynamic boundary element method for modeling rockbursts. Proc. of 2nd Int. Symp. on Rockbursts and Seismicity in Mines. Balkema, pp 93–99

Madariaga R (1976) Dynamics of an expanding circular fault. B Seismol Soc Am 66(3): 639–666

Marti J, Cundall PA (1982) Mixed discretization procedure for accurate modelling of plastic collapse. Int J Numer Anal Met Geomech 6: 129–139

McGarr A (1993) Keynote address: factors influencing the strong ground motion from mining-induced tremors. In: Young RP (ed) Proc. of 3rd Int. Symp. on Rockbursts and Seismicity in Mines. Balkema, pp 3–12

McGarr A (1997) A mechanism for high wall-rock velocities in rockbursts. Pure Appl Geophys 150: 381–391

Milev AM, Spottiswoode SM, Stewart RD (1999) Dynamic response of the rock surrounding deep level mining excavations. Proc. of 9th ISRM Int. Congress on Rock Mech. Paris, pp 1109–1114

Molenkamp F, Kidger DJ, Smith IM (1992) Accuracy of four-node standard finite element. Int J Numer Anal Met 16: 323–333

Müller W (1991) Numerical simulation of rockbursts. Mining science and technology, vol. 12, pp 27–42

Myer LR, Hopkins D, Cook NGW (1985) Effect of contact area of an interface on acoustic wave transmission characteristics. Proc. of 26th US Symp. on Rock Mech. Balkema, pp 565–572

Myer LR, Hopkins D, Peterson JE, Cook NGW (1995) Seismic wave propagation across multiple fractures. In: Myer LR, Cook NGW, Goodman RE, Tsang P (eds) Fractured and jointed rock masses. Balkema, pp 105–109

Napier JAL, Hildyard MW (1992) Simulation of fracture growth around openings in highly stressed brittle rock. J South African Inst Min Metall 6: 159–168

O'Connell RJ, Budiansky B (1974) Seismic velocities in dry and saturated cracked solids. J Geophys Res 79: 5412–5426

Ortlepp WD (1993) High ground displacement velocities associated with rockburst damage. In: Young RP (ed) Proc. of 3rd Int. Symp. on Rockbursts and Seismicity in Mines. Balkema, pp 101–106

Pyrak-Nolte LJ, Myer LR, Cook NGW (1990a) Transmission of seismic waves across single natural fractures. J Geophys Res 95(B6): 8617–8638

Pyrak-Nolte LJ, Myer LR, Cook NGW (1990b) Anisotropy in seismic velocities and amplitudes from multiple parallel fractures. J Geophys Res 95(B7): 11345–11358

Rockfield Software Ltd (1999) ELFEN user manual v.2.8. University College of Swansea
Sayers CM, Kachanov M (1991) A simple technique for finding effective elastic-constants of cracked solids for arbitrary crack orientation statistics. Int J Solids Structures 27(6): 671–680
Schoenberg M (1980) Elastic wave behaviour across linear slip interfaces. J Acoust Soc Am 68(5): 1516–1521
Siebrits E, Hildyard MW, Hemp DA (1993) Stability of backfilled stopes under dynamic excitation. In: Young RP (ed) Proc. of 3rd Int. Symp. on Rockbursts and Seismicity in Mines. Balkema, pp 117–121
Spottiswoode SM, Durrheim RJ, Vakalisa B, Milev AM (1997) Influence of fracturing and support on the site response in deep tabular stopes. Proc. of 1st Southern African Rock Engineering Symposium (SARES). Johannesburg, South Africa, pp 62–67
Tinucci JP, Spearing AJS (1993) Strategies for clamping faults and dykes in high seismicity tabular mining conditions. In: Young RP (ed) Proc. of 3rd Int. Symp. on Rockbursts and Seismicity in Mines. Balkema, pp 435–440
Uenishi K (1997) Rayleigh pulse dynamic triggering of interface slip. PhD Thesis, Vienna University of Technology, pp 1–178
Virieux J (1984) SH-wave propagation in heterogeneous media: velocity-stress finite-difference method. Geophysics 49(4): 1933–1957